HHS Public Access

Author manuscript

Nat Mater. Author manuscript; available in PMC 2022 March 14.

Published in final edited form as:

Nat Mater. 2016 January ; 15(1): 106–112. doi:10.1038/nmat4421.

Topological Defects in Liquid Crystals as Templates for Molecular Self-Assembly

Xiaoguang Wang[1], **Daniel S. Miller**[1], **Emre Bukusoglu**[1], **Juan J. de Pablo**[2], **Nicholas L. Abbott**[1,*]

[1]Department of Chemical and Biological Engineering, University of Wisconsin-Madison, Madison, WI 53706-1691 USA

[2]Institute for Molecular Engineering, University of Chicago, Chicago, Illinois 60637 USA

Abstract

Topological defects in liquid crystals (LCs) have been widely used to organize colloidal dispersions and template polymerization, leading to a range of assemblies, elastomers and gels. However, little is understood about molecular-level assembly processes within defects. Here, we report that nanoscopic environments defined by LC topological defects can selectively trigger processes of molecular self-assembly. By using fluorescence microscopy, cryogenic transmission electron microscopy and super-resolution optical microscopy, we observed signatures of molecular self-assembly of amphiphilic molecules in topological defects, including cooperativity, reversibility and controlled growth. We also show that nanoscopic o-rings synthesized from Saturn-ring disclinations and other molecular assemblies templated by defects can be preserved by using photocrosslinkable amphiphiles. Our results reveal that, in analogy to other classes of macromolecular templates such as polymer-surfactant complexes, topological defects in LCs are a versatile class of three-dimensional, dynamic and reconfigurable templates that can direct processes of molecular self-assembly.

Keywords

liquid crystal; molecular self-assembly; topological defects; amphiphiles

*To whom correspondence may be addressed: abbott@engr.wisc.edu.

Additional Information

Additional information can be found in Supplementary Information, which includes: exposure times used in fluorescence microscopy; absorption and emission properties of BODIPY-labeled amphiphiles; proportionality of rescaled fluorescence intensity to exposure time and concentration of fluorophore; distribution of BODIPY into LCs; distribution of BODIPY-DHPE into LCs; contribution of "core replacement" to ΔG_1^0; contribution of interfacial tension to ΔG_1^0; reversible assembly and disassembly of amphiphilic molecules in LC defects; thermodynamic model for molecular self-assembly in LC defects.

Author Contribution

X.W., J.D.P and N.L.A. designed the experiments. X.W., D.S.M. and E.B. performed the experimental work. X.W. and N.L.A. analyzed the data. X.W., D.S.M., J.D.P and N.L.A. wrote the paper. N.L.A. supervised the research. All authors discussed the progress of research and reviewed the manuscript.

The presence of structural and dynamical heterogeneity within both hard and soft materials has profound effects on mechanical[1,2], thermal[2–4] and optical properties[4,5]. Within soft matter systems comprising liquid crystals (LCs), for example, topological defects have been shown to direct the assembly of metallic nanoparticles into chains with unusual plasmonic properties[6,7], to lead to the gelation of colloidal dispersions[8,9] or, in defect-rich phases such as so-called blue phases, to permit the synthesis of responsive optical elastomers via polymerization[10–12]. Although the promise of defect-directed LC materials on the meso-scale is illustrated by these prior studies, the possibility of using the nanoscopic environments created by defects within LCs to direct the reversible formation of well-defined assemblies of molecules has not been explored. We hypothesized that selective formation of molecular assemblies within the nanoscopic cores of defects may be possible because the ordering of the mesogens within singular defects is diminished relative to the bulk LC and thus the physical properties of defects are distinct from the bulk material.

The spontaneous self-assembly of molecules into nanoscopic structures has been employed to realize a diverse range of bulk and interfacial properties of soft materials[13–15]. A signature of molecular self-assembly is “cooperative” self-association, which arises because thermodynamic stabilization of the assembled structure requires participation of a threshold number of building blocks[13]. In addition, self-assembly is characterized by reversibility (leading to high levels of perfection) and formation of nanostructures of well-defined size (in contrast to uncontrolled aggregation or phase separation processes). More recently, hierarchical self-assembly[13,14], involving self-association on multiple length-scales, as well as directed self-assembly[13,15], employing external constraints (e.g., fields or chemical templates) to guide assembly pathways, have been explored to achieve multilevel control of the organization (e.g., spatial control) of self-assembled systems. In this paper, we report the discovery that processes of molecular self-assembly can be triggered and directed by the local environments of topological defects formed in thermotropic LCs, thus unmasking the basis of a broad and versatile new class of three-dimensional templates for the design of self-assembled molecular materials.

The molecules (mesogens) within the bulk of a nematic LC exhibit long-range orientational order, which is typically characterized by the so-called director (the average orientation of the molecules within a small volume of the LC). Topological defects form in LCs when internal constraints (e.g., the presence of chiral dopants leading to blue phases) or external boundary conditions (e.g., the anchoring of LC on the internal surface of a cavity) cannot be satisfied by continuous strain of the LC director via bend, twist or splay[16]. The sizes and shapes of topological defects formed within LCs can range from points to walls to lines, all of which can be precisely generated in three-dimensions in a predictable manner and also manipulated using external fields[16]. For example, and of particular relevance to the study reported in this paper, singular line defects (disclinations) can form near the equator of solid particles that anchor a nematic LC in a perpendicular (homeotropic) orientation (the line defect resembles a “Saturn-ring”[17]), or knotted and kinked line defects can be formed around particles in chiral nematic phases[18,19]. The orientational order of mesogens within a LC gradually decreases when moving from the bulk of a LC to the core of a singular topological defect, leading to local changes in the physical properties of the LC. The diameter of the core region of a singular defect in a nematic LC, within which the free

energy density is higher than the bulk LC[20], can be estimated as $d_c \sim (K/\varepsilon)^{1/2}$, where K is the elastic constant of the LC and ε is the free energy of disordering the nematic phase. A typical value for d_c is ~ 10 nm. More detailed and complete descriptions of defects, based on the tensorial order parameter, Q_{ij}, describe the continuous change in the orientational order of mesogens between the core of the defect and the bulk of the LC[21]. Experiments described below reveal that the characteristic disorder of mesogens within the nanoscopic cores of topological defects in LCs can guide processes of molecular self-assembly involving amphiphiles, and that the defects do so in a manner that is strongly analogous to cooperative association of amphiphiles in other broad classes of complex fluids (e.g., aqueous solution of amphiphiles and associative polymers[22–28]). Because LC defects can be formed reversibly, can be manipulated with external fields, and can exhibit a wide-range of complex topologies, the results in this paper reveal a new and versatile class of templates for the synthesis of self-assembled molecular structures.

Formation of defects in liquid crystals

Singular disclinations of strength −1/2 (line defects) were generated by dispersing silica microparticles (diameters of 68 ± 4 μm, treated with octyltrichlorosilane (OTS) to cause perpendicular anchoring of nematic LCs) in an isotropic phase of 4-cyano-4′-pentylbiphenyl (5CB) that contained a predetermined concentration of an amphiphile. This mixture was confined between two polyimide-coated glass slides that were rubbed and oriented so as to induce a 90° twist within the 5CB when cooled into the nematic phase. The twist within the LC, when combined with the perpendicular orientation of the LC on the surfaces of the microparticles, generated −1/2 line defects around and between the silica particles[18], as shown in Fig. 1a and b. Our initial observations were based on regions of the defect lines that were located between the colloids (see box in Fig. 1b). We used amphiphiles labeled with dipyrromethene boron difluoride (BODIPY) in our initial experiments because the fluorescence emission of BODIPY-labeled amphiphiles changes upon self-association of the amphiphiles[29]. As detailed in the Supplementary Information, excitation at 457–502 nm and quantification of emission at 510–562 nm permitted imaging of monomeric (singly dispersed) BODIPY amphiphiles in the 5CB, whereas excitation at 533–584 nm and emission at 606–684 nm yields a strong signal from self-assembled amphiphiles (so-called dimer signal; see below for additional discussion). We note that light emitted by monomers is absorbed negligibly by dimers in our system due to the low concentrations of dimers (see Supplementary Information). For the measurements reported in this paper, we confirmed that the fluorescence intensity was linearly proportional to both exposure time and concentration of BODIPY in the absence of self-association (Supplementary Information and Fig. S3).

Cooperative self-association of amphiphiles in LC defects

First, we characterized the interaction of BODIPY alone (not conjugated to an amphiphile) with a −1/2 line defect in nematic 5CB. The line defect was readily located using bright field optical imaging, as shown in Fig. 2a. Inspection of Fig. 2b and c reveals, however, no measurable difference between the fluorescence intensity of the defect and the bulk of the nematic phase (under both imaging conditions mentioned above), a result that we confirmed

over a wide range of BODIPY concentrations (10 – 950 μM; Fig. S3). This result indicates that BODIPY alone does not measurably partition to the defect relative to the bulk LC, which is in striking contrast to the behavior of the amphiphiles reported below.

Next, we imaged amphiphiles comprised of fatty acids (with various chain lengths; C5 to C16) conjugated to BODIPY that were dissolved into nematic LC containing −1/2 line defects. We focus here on the results obtained using BODIPY-C5 (Fig. 1c), as an example that is representative of all BODIPY conjugates of fatty acids used in this study. For concentrations of BODIPY-C5 up to 57 μM (see Supplementary Information), independent of the excitation/emission wavelengths used for imaging (see above), we measured no difference between the fluorescence intensity of the −1/2 defects and bulk LC (similar to BODIPY only, see Fig. 2a–c). When the concentration of BODIPY-C5 was 59 μM or higher, however, the fluorescence from dimeric (Fig. 2f) but not monomeric BODIPY-C5 (Fig. 2e) was more intense in the defect relative to the bulk of the LC. Furthermore, quantification of the fluorescence intensity revealed a clear break in a plot of BODIPY dimer fluorescence versus concentration (Fig. 2h) at 59 μM. We note that the apparent non-zero dimer fluorescence intensity measured in the bulk LC above and below 59 μM is a background signal generated by monomers (due to overlap of the absorption/emission bands; see Supplementary Information). Overall, the results above hint that BODIPY-C5, above a threshold concentration (critical assembly concentration (CAC)) of 59 μM, associates within the local environment of the defect while remaining singly dispersed in the bulk of the LC. As shown in Fig. 2h, similar behaviors were observed for BODIPY-C12 and BODIPY-C16, with the difference that the CAC of each amphiphile (corresponding to the onset of self-association in the defect) was observed to decrease with increase in tail length. Because the spatial resolution of the images in Fig. 2a–f is limited by the diffraction of light, we also used super-resolution optical microscopy (STORM) to image ATTO 488-labeled amphiphiles in the −1/2 defects. These studies revealed molecular assemblies with apparent widths less than 80 nm (see Methods for details), although motion of the defect during imaging contributed to this apparent size (see below for cryogenic transmission electron micrographs (cryo-TEM) that reveal the mean diameters of the assemblies to be 28 nm). We comment here also that the formation of amphiphilic assemblies in −1/2 defect lines did not lead to measurable changes in the orientations of the LC in the surrounding sample.

Controlled growth of molecular assemblies in LC defects

The above-described observation of a chain-length-dependent CAC is consistent with the self-assembly of amphiphiles within the LC defects under conditions during which the amphiphiles remain singly dispersed in the bulk LC. We emphasize that this physical phenomenon contrasts to past reports of the partitioning of preformed particles/polymers from bulk LCs into defects[30–37], where the particles/polymers were present within both the bulk LC and defect. To provide additional support for our proposal that amphiphilic assemblies are forming selectively within the nanoscopic environment of the LC defects (and not in the bulk), we examined the state of dispersion of the BODIPY-labeled amphiphiles in the bulk LC over a wide range of concentrations. The results in Fig. 3a confirm that the fluorescence intensity of each BODIPY-fatty acid in bulk LC increased linearly (without any sign of a “break” in the dimer signal) up to 950 μM (a concentration

that is at least an order of magnitude higher than the CAC of each amphiphile within the −1/2 LC defect). This result provides further support for our conclusion that the self-assembly of the amphiphiles is triggered by the environment of the LC defects.

As noted above, processes of molecular self-assembly are distinguished from aggregation and bulk phase separation by the controlled growth of the assemblies after the onset of self-association (in contrast, a bulk phase separation continues until macroscopic segregation has taken place). To this end, we characterized the self-association of BODIPY-labeled amphiphiles in LC defects at concentrations that exceeded the CACs reported above. Inspection of Fig. 3b reveals that the fluorescence generated by amphiphiles assembled within a −1/2 line defect increased steeply up to a threshold concentration above which the rate of change of the fluorescence intensity greatly diminished, a signature that is consistent with a controlled mode of growth. We also note that the threshold concentration at which the initial growth rate ceased was observed to decrease with increase in the amphiphile tail length (see inset in Fig. 3b). Further evidence of formation of controlled assemblies was obtained by using cryo-TEM. In these experiments, we used blue phase LCs to obtain a sufficiently high density of −1/2 disclination lines to allow imaging by cryo-TEM (see Methods). Fig. 3c shows an electron micrograph of an amphiphilic assembly formed by the phospholipid PC-C12 (see Fig. 1 for the structure of PC-C12). The mean diameter of the assembly was measured to be 28 ± 4 nm (see Fig. 3d for a histogram of diameters), corresponding to the thickness of approximately 9 lipid bilayers[38] (see below for additional discussion of the internal organization of these assemblies). In contrast, the past reports of the partitioning of preformed particles/polymer to defects have described uncontrolled growth of aggregates into the micrometer to millimeter size range[29–36].

Thermodynamics of molecular self-assembly in LC defects

Overall, three key results reported above – namely (i) the observation of chain-length-dependent CACs of amphiphiles in defects, (ii) the absence of self-association of amphiphiles in bulk LC, and (iii) formation of assemblies of controlled size in defects – support our conclusion that defects in LCs can trigger amphiphiles to form self-assembled nanostructures. These key signatures of self-assembly were also observed for a range of other phospholipids with varying head groups and aliphatic tail lengths (see Fig. 1d for molecular structures of the phospholipids; see Methods for details), revealing the generality of the phenomenon. For all of these amphiphiles, we calculated the change in standard free energy accompanying the transfer of one amphiphile from a monomeric (singly-dispersed) state in the bulk LC phase to the assembled state within the environment of the LC defect using $\Delta G_1^0 = k_B T ln CAC$[39] (see Supplementary Information). As shown in Fig. 4, ΔG_1^0 calculated as a function of the amphiphile tail length from measured values of the CAC yielded a linear relationship. Specifically, the slope of the plot reveals that the driving forces for self-association of the amphiphiles within the defects increased by 0.13 $k_B T$ per methylene unit of the tail. The intercepts of the best-fit lines for the distinct families of amphiphiles (Fig. 4) reveal that the head groups (e.g., zwitterionic versus non-ionic) also contribute to the standard free energy of self-association in the defects (see also inset in Fig. 4).

The results shown in Fig. 4 are strikingly similar to past studies of the self-assembly of amphiphiles in aqueous solutions, where the driving force for self-assembly also increases in proportion to the tail length of the amphiphile[40]. Quantitatively, however, the contribution of the tails to the driving force leading to self-assembly in LC defects (0.13 k_BT/methylene) is weaker than that for aqueous solutions (around 0.69 k_BT/methylene [40]). In aqueous solutions, the driving force is largely entropic in origin, arising from the release of structured water around the hydrocarbon chains of amphiphiles upon their self-association. Because a nematic LC is also a structured solvent, we hypothesized that the self-assembly of amphiphiles in LC defects may also be largely entropically driven. Specifically, for low molecular weight mesogens with flexible alkyl tails, it is known that the conformational degrees of freedom of the alkyl chains increase during a phase transition from a nematic to an isotropic state. The gain in conformational entropy is estimated to be ~ 0.18 k_BT/methylene[41], which is comparable in magnitude to the tail length-dependent contribution that we estimate from our experiments (0.13 k_BT/methylene, Fig. 4). We note, however, that the tails of the amphiphiles within lipid assemblies must also satisfy packing constraints[42]. In addition, the formation of the lipid assembly within the core of the defect results in the transfer of mesogens from the disordered core to the bulk LC. We estimate this "core displacement" contribution to be 0.04 k_BT/methylene of the amphiphile tail, or 10^3 k_BT per 10 nm length of the assembly formed in the LC defect (see Supplementary Information).

Our observations of cooperative self-assembly of amphiphiles within the nanoscopic environments of LC defects reveal striking similarities to the self-association of amphiphiles with polymers in aqueous solvents (such as hydrophobically-modified polymers)[24–28]. When surfactant molecules are introduced into an aqueous solution of an associating polymer (e.g., with hydrophobic side-chains), the surfactants bind cooperatively to the polymer to form mixed micelles, resulting in a CAC that is lower than the CAC of surfactant alone[22–28]. In our LC system, the defects assume a role that is analogous to an associative polymer, and cooperative association of amphiphiles within LC defects is driven by the free energy gain associated with simultaneous formation of an amphiphilic assembly and elimination of the high free energy cores of the LC defects (see above). We hypothesized that a classical model of cooperative self-assembly of amphiphiles with polymers would also describe the essential change in the concentration-dependent monomer and dimer signals shown in Figure 4a and b (see Supplementary Information)[43–45]. According to this model, the concentrations of amphiphiles in singly dispersed and assembled states are related by:

$$[X_{total}] = [X_1] + [X_{defect}] = [X_1] + \sum_{n=1}^{m} \frac{g_d[X_d]}{m} \frac{k_{d,n}[X_1]^{g_d}}{1 + k_{d,n}[X_1]^{g_d}} \quad (1)$$

where $g_d[X_d]$ is the concentration of amphiphiles self-assembled in the defects, $k_{d,n}$ are the intrinsic equilibrium constants characterizing self-assembly of the amphiphiles in the defects, and $[X_{total}]$, $[X_1]$ and $[X_{defect}]$ are the concentrations of all amphiphiles, singly dispersed amphiphiles, and assembled amphiphiles, respectively (see Supplementary Information for detailed derivations, and discussion of $[X_d]$, g_d and $k_{d,n}$). As shown by the red curve in Fig. 3e, this simple model predicts a linear increase in $[X_1]$ with $[X_{total}]$, consistent with our experimental observations. Furthermore, as shown by the blue curve in

Fig. 3e, the model predicts the increase of [X_{defect}] above the CAC until the defects become saturated. We also note that in aqueous solutions of associating polymers, amphiphiles typically exhibit a second CAC corresponding to the onset of association of polymer-free amphiphiles[22–28]. Consistent with this observation, by using lipids with sufficiently long tails (e.g., BODIPY-DHPE, Fig. 1c), we also observed amphiphiles to exhibit a first CAC in the defects and a second CAC in the bulk LC (see Fig. 2i and Supplementary Information).

Polymerization of molecular assemblies in LC defects

Topological defects are a particularly promising class of templates for directing the self-assembly of amphiphiles because they can be formed with remarkable precision and complexity, and because they can be formed reversibly. For example, Fig. 5a–e show the formation and erasure of a −1/2 line defect near the equator of a microparticle dispersed in a nematic LC (a “Saturn-ring” defect). The reversible assembly and disassembly of amphiphilic molecules within the defect is shown to follow the formation and erasure of the disclination line (by heating from 25 °C to 38 °C; see Methods). By using a photoreactive lipid (1,2-bis(10,12-tricosadiynoyl)-sn-glycero-3-phosphoethanolamine (diyne PC); see Methods), we also demonstrated that the lipid assembly formed within the “Saturn-ring” defect can be transformed into a free standing polymeric ring. Specifically, following photocrosslinking of diyne PC and heating of the LC above the clearing temperature, we observed the polymeric “o-ring” with a cross-section of 20 nm (see Fig. 5g) to slip from the equatorial plane of the microparticle, as shown in Fig. 5f. TEM of the polymeric structure in Fig. 5g revealed well-defined lamellae (the dark regions are the head groups), with a periodicity consistent with the presence of 5 lipid bilayers. We note here that the polymerizable lipids (diyne PC) used in this study have been reported previously to form layered assemblies in aqueous phases[46].

Overall, the results presented in this paper support our hypothesis that the local nanoenvironments created by singular topological defects formed in LCs can be used to trigger and template cooperative processes involving the self-assembly of molecular amphiphiles, as shown in Figure 6. This finding expands the potential utility of defects for materials synthesis into the realm of molecules and nanoscopic molecular assemblies. We note that past studies of polymer-stabilized blue phases have used monomers with flexible alkyl chains[10,11,47], which our results suggest may also drive their partitioning into the defect regions for photopolymerization. We note also that the results reported in this paper provide further insight into our recent observations that bacterial endotoxins can trigger configurational transitions in micrometer-sized LC droplets at extraordinarily low concentrations by accumulating at LC defects[48,49]. Future efforts will seek to use polarized STORM and fluorescence confocal microscopy to provide insight into molecular orientations within self-assembled nanostructures formed in LC defects. In addition, the influence of molecular assemblies on the annihilation of oppositely charged defects is being investigated.

Methods

Materials

The following fluorescent compounds were purchased from Molecular Probes: 4,4-difluoro-1,3,5,7-tetramethyl-4-bora-3a,4a-diaza-s-indacene (BODIPY), 4,4-difluoro-5,7-dimethyl-4-bora-3a,4a-diaza-s-indacene-3-pentanoic acid (BODIPY-C5), 4,4-difluoro-5,7-dimethyl-4-bora-3a,4a-diaza-s-indacene-3- dodecanoic acid, (BODIPY-C12), 4,4-difluoro-5,7-dimethyl-4-bora-3a,4a-diaza-s- indacene-3-hexadecanoic acid (BODIPY-C16), and N-(4,4-difluoro-5,7-dimethyl-4- bora-3a,4a-diaza-s-indacene-3-propionyl)-1,2-dihexadecanoyl-*sn*-glycero-3-phosphoe thanol-amine triethylammonium salt (BODIPY-DHPE). The following phospholipids were purchased from Avanti Polar Lipids, Inc.: 1,2-dipropionyl-*sn*-glycero-3-phosphocholine (PC-C3), 1,2-dihexanoyl-sn-glycero-3- phosphocholine (PC-C6), 1,2-dilauroyl-sn-glycero-3-phosphocholine (PC-C12), 1,2-distearoyl-sn-glycero-3-phosphocholine (PC-C18), and 1,2-dilignoceroyl-*sn*-glycero-3-phosphocholine (PC-C24), 1,2-dilauroyl-*sn*-glycero-3-phosphate sodium salt (PA-C12), 1,2-dilauroyl-sn-glycero-3-phosphoethanolamine (PE-C12), 1,2-dilauroyl-sn-glycero-3-phospho-(1′-rac-glycerol) sodium salt (PG-C12), 1,2-dilauroyl-*sn*-glycero-3-phospho-L-serine sodium salt (PS-C12), 1,2-bis(10,12-tricosadiynoyl)-*sn*-glycero-3-phosphocholine (diyne PC; polymerizable lipid). ATTO 488-labeled 1,2-ditetradecanoyl-*sn*-glycero-3-phosphoethanolamine (ATTO 488-PE-C14) for super-resolution optical microscope (STORM) characterization was purchased from ATTO-TEC GmbH. Copper grids coated with ~ 5 nm-thick carbon film for transmission electron microscopy (TEM) were purchased from Electron Microscopy Sciences. Ethanol (anhydrous) was purchased from Pharmco-AAPER. Chloroform and octyltrichlorosilane (OTS) were obtained from Sigma-Aldrich. Heptane was purchased from Fisher Scientific. Dichloromethane was purchased from ACROS Organics. Nematic liquid crystal (LC) 4′-pentyl-cyanobiphenyl (5CB), MLC-2142 and the chiral dopant S-811 (used to prepare blue phase LCs) were purchased from EMD chemicals. Polyimide (PI 2556) was purchased from HD Microsystems. Fisher's Finest Premium Grade glass microscope slides and #1.5 coverslips were obtained from Fisher Scientific. Monodisperse silica microparticles with diameter 68 ± 4 μm were purchased from Particle Technology Ltd.

Preparation of polyimide-coated glass slides

A spin coater (WS-400A-6NPP/Lite, Laurell Technologies) was used to coat glass slides with a polyimide solution. The coated slides were then heated on hot plate at 70°C for 2 min to evaporate the solvent, and subsequently placed in an oven at 200°C for 2 hrs. Finally, the slides were cooled to room temperature (~ 25°C), and rubbed in a single direction at 10 inches/min for 1 min by satin cloth to induce an alignment of LC parallel to the direction of rubbing.

Preparation of OTS-coated silica microparticles

10 mg silica microparticles were rinsed with deionized water three times, and then added to an OTS-heptane solution (1.2×10^{-2} % v/v) with stirring. Stirring was continued for 45 min. Finally, the microparticles were rinsed with dichloromethane three times and dried with nitrogen.

Preparation of mixtures of BODIPY-amphiphiles and 5CB

Here we describe the procedure used to prepare a mixture of BODIPY-C5 (19 μM) in 5CB. Similar procedures were used to prepare mixtures of other BODIPY-amphiphiles and 5CB. First, 0.3 μL of 1 mg/mL BODIPY-C5 in ethanol was added to 30 μL of chloroform. Then, 50 μL of 5CB was added to the BODIPY-C5 chloroform solution. The mixture was sonicated for 3 min and then dried under vacuum at 45°C for 30 min to remove the ethanol and chloroform. Following drying, the mixture of BODIPY-C5 and 5CB was kept in the isotropic phase (at 45°C) prior to injection into an optical cell.

Fabrication of optical cells

Optical cells were prepared by pairing two polyimide-coated glass slides and spacing them apart using OTS-coated microparticles. The alignment/rubbing directions of the polyimide in the top and bottom glass slides were set at 90° to induce a twist deformation into the bulk LC, which favors formation of knotted and kinked line defects around particles[18]. The mixture of BODIPY-amphiphile and 5CB (in the isotropic phase) was injected into the optical cell and then cooled into the nematic phase at room temperature.

UV-vis spectrophotometer measurement

The absorbance and emission spectra of BODIPY-amphiphiles were measured by using a Tecan Infinite M1000 plate reader. The measurements were taken in black, flat, clear bottom 96-well plates (Corning Inc.).

Fluorescence microscopy of BODIPY-labeled amphiphiles in 5CB

The distribution of BODIPY-amphiphiles in 5CB was characterized by inverted fluorescence microscopy using an Olympus IX71 microscope with a 100 W mercury lamp. The fluorescence filter sets used in the experiments were purchased from Chroma Inc. Images were collected with a Hamamatsu 1394 ORCA-ER CCD camera connected to a computer and controlled through Simple PCI imaging software (Compix Inc.). Filter set 1 was comprised of an excitation filter that transmitted light with wavelengths between 457 nm and 502 nm (λ^{ex}: 457–502 nm) and an emission filter that transmitted light with wavelengths of 510 nm to 562 nm (λ^{em}: 510–562 nm). Filter set 2 used excitation and emission filters that transmitted light with wavelengths of 533 nm to 584 nm (λ^{ex}: 533–584 nm) and 606 nm to 684 nm (λ^{em}: 606–684 nm), respectively. Within the range of wavelengths of light transmitted by the excitation filters, the white light from the mercury lamp exhibits peaks in emission at 490 nm, 546 nm and 579 nm.

Quantification of fluorescence intensity

The fluorescence intensity of the BODIPY-amphiphiles was quantified from images using ImageJ software. Here we briefly describe our methods with reference to Fig. S1 in the Supplementary Information. Fig. S1a and b show bright field and corresponding fluorescence micrographs of a −1/2 disclination line in a LC film that contained 1.9 μM BODIPY-DHPE. For quantification of the fluorescence from the defect, we used the “threshold” function to select the region encompassing the line defect in the bright field micrograph. In all the measurements reported in this paper, we consistently set the lower

limit of the “threshold” to 0, and the upper limit to 185–195. The result of the “threshold” selection is shown in Fig. S1c. The region identified in the bright field image to contain the defect (Fig. S1c) was used to define the region in the fluorescence micrograph in which the fluorescence intensity was quantified (Fig. S1d). This procedure permitted consistent quantification of the fluorescence intensity within −1/2 disclination lines. In a final step, we selected a region of the bulk LC adjacent to the defect line for quantification of the fluorescence intensity of the bulk LC (Fig. S1e). The rescaled fluorescent intensity was calculated as:

$$rescaled\ fluo\ intensity = \frac{1\ s}{actual\ exposure\ time} \times measured\ grayscale \tag{2}$$

Fluorescence microscopy of phospholipids in LCs

Mixtures of phospholipids and 5CB were prepared by using procedures similar to those used to prepare mixtures of BODIPY-amphiphiles and 5CB (see above). To permit fluorescence imaging of the phospholipid assemblies, we doped BODIPY-C5 (~ 3 % mol/mol based on the phospholipids) into the mixture of phospholipids and 5CB. Here we make three comments that guided this approach. First, no detectable fluorescence signal was observed when using pure phospholipids in LCs (in the absence of BODIPY-C5) over the concentration range used in the present study. Second, the concentration of doped BODIPY-C5 was always at least one order of magnitude below its critical association concentration (CAC; 59 μM) to avoid formation of assemblies of BODIPY-C5. Third, when the concentration of phospholipid was above its CAC, we measured the monomeric signal (λ^{em} 510–562 nm) but not the dimeric signal (λ^{em} 606–684 nm) to increase in the LC defects relative to the bulk LC (in the presence of the BODIPY-C5). This result indicates that the dilution of BODIPY-C5 into the phospholipid assembly prevents substantial dimer signal (see Supplementary Information for details on BODIPY dimer signal)[29]. Thus, we used the change in the monomeric signal (λ^{em} 510–562 nm) from the BODIPY-C5 to indicate the CAC of the phospholipids in the defects.

Super-resolution optical microscopy (STORM)

Mixtures of PC-C12 (19 μM) and 5CB were used for STORM. ATTO 488-labeled PE-C14 (10 % mol/mol based on PC-C12) was also doped into the mixture as a fluorescent probe for STORM imaging[50]. Optical cells were prepared by using polyimide-coated #1.5 coverslips. Imaging was carried out on a Nikon N-STORM inverted TIRF microscope with 405 nm and 488 nm laser excitation. Images were collected with an Andor iXon Ultra 897 EMCCD camera and controlled through NIS-Elements Ar software with N-STORM analysis. Images were acquired after an initial 1 min pre-exposure (to allow the transition of the majority of fluorophores into a meta-stable dark state) followed by a 5–10 min acquisition period at 17 ms/frame. The apparent widths of the assemblies formed in LC defects were determined by measuring the full width at half maximum (FWHM) of the assemblies.

Cryo-TEM of amphiphilic assemblies

Our approach to imaging of phospholipid assemblies in blue phase LCs was guided by past studies that have reported the use of cryo-TEM for characterization of a range of self-assembled nanostructures in oils[51–55]. Blue phase LCs were prepared by mixing MLC-2142 with 35 % wt/wt chiral dopant S-811. Next, 0.01 % wt/wt PC-C12 (based on blue phase LC mass) was added to the MLC-2142/S-811 mixture using procedures described above in the context of preparing mixtures of phospholipid and 5CB (see above). The LC mixture was held at 46°C (blue phase temperature range is between 44–48°C) for 10 min and then vitrified in liquid nitrogen by using a FEI Vitrobot. Subsequently, cryogenic sectioning was performed at −120°C by using a Diatome cryo-diamond knife mounted on a Leica ultramicrotome with cryogenic sectioning capability. The slice thickness was set to 80–100 nm. The microtomed samples were then transferred onto carbon film-coated TEM grids. Cryo-TEM imaging was carried out on a Tecnai 12 TEM with cryogenic capability. The TEM imaging was operated at 120 kV. A Gatan cryo-TEM holder was used to keep the sample below −170°C during cryo-TEM imaging. The TEM images were collected on a Gatan ultrascan CCD camera.

Crosslinking of lipids in LC defects

A mixture of crosslinkable lipid (diyne PC, 20 μM) with 5CB was prepared using procedures described above. In brief, 8 μL of 0.1 mg/mL diyne PC in ethanol was mixed with 30 μL of chloroform and 50 μL of 5CB. BODIPY-C5 (2 % mol/mol based on diyne PC) was added as a fluorescent probe. The mixture was sonicated for 30 s and then placed in a vacuum oven at 38°C for 30 min to remove the ethanol and chloroform. Subsequently, the mixture was introduced into an optical cell along with OTS-treated microspheres (see above). The directions of rubbing of the polyimide coatings on the glass microscope slides that were used to form the optical cells were parallel. “Saturn-ring” defects were observed to form near the equator of the particles[17]. The optical cells were exposed to UV light (254 nm) for 30 min to crosslink diyne PC[46]. Similarly, as detailed above, monomeric signal λ^{em} 510–562 nm was used to localize the assemblies formed by diyne PC. We comment here that prior to polymerization, reversible assembly and disassembly of the amphiphilic assemblies was achieved by reversible formation and erasure of disclinations (by heating from 25°C to 38°C; the clearing temperature of 5CB is ~ 35°C; see Fig. 5a–e in the main text). Following the crosslinking and heating of the LC above the clearing temperature, the polymeric assemblies did not disassemble and they were transferred to carbon film-coated grids for further TEM characterization, as shown in Fig. 5f and g.

Supplementary Material

Refer to Web version on PubMed Central for supplementary material.

Acknowledgments

This work was supported by the National Science Foundation (under awards DMR-1121288 (MRSEC) and CBET-1263970), the Army Research Office (W911-NF-11-1-0251 and W911-NF-14-1-0140), and the National Institutes of Health (CA108467 and AI092004). STORM imaging and analysis was performed at the Biochemistry Optical Core, University of Wisconsin-Madison.

References

1. Alden JS, Tsen AW, Huang PY, Hovden R, Brown L, Park J, Muller DA, McEuen PL. Strain solitons and topological defects in bilayer graphene. Natl Acad Sci U S A. 110: 11256–11260. 2013.
2. Lu K, Lu L, Suresh S. Strengthening materials by engineering coherent internal boundaries at the nanoscale. Science. 324: 349–352. 2009. [PubMed: 19372422]
3. Weber CA, Bock C, Frey E. Defect-mediated phase transitions in active soft matter. Phys Rev Lett. 112: 168301. 2014; [PubMed: 24815670]
4. Sachet E, Shelton CT, Harris JS, Gaddy BE, Irving DL, Curtarolo S, Donovan BF, Hopkins PE, Sharma PA, Sharma AL, Ihlefeld J, Franzen S, Maria J. Dysprosium-doped cadmium oxide as a gateway material for mid-infrared plasmonics. Nature Mater. 14: 414–420. 2015. [PubMed: 25686264]
5. van der Zande AM, Huang PY, Chenet DA, Berkelbach TC, You Y, Lee G, Heinz TF, Reichman DR, Muller DA, Hone JC. Grains and grain boundaries in highly crystalline monolayer molybdenum disulphide. Nature Mater. 12: 554–561. 2013. [PubMed: 23644523]
6. Liu Q, Cui Y, Gardner D, Li X, He S, Smalyukh II. Self-alignment of plasmonic gold nanorods in reconfigurable anisotropic fluids for tunable bulk metamaterial applications. Nano Lett. 10: 1347–1353. 2010. [PubMed: 20334353]
7. Dickson W, Wurtz GA, Evans PR, Pollard RJ, Zayats AV. Electronically controlled surface plasmon dispersion and optical transmission through metallic hole arrays using liquid crystal. Nano Lett. 8: 281–286. 2008. [PubMed: 18085813]
8. Wood TA, Lintuvuori JS, Schofield AB, Marenduzzo D, Poon WCK. A self-quenched defect glass in a colloid-nematic liquid crystal composite. Science. 334: 79–83. 2011. [PubMed: 21980107]
9. Bukusoglu E, Pal SK, de Pablo JJ, Abbott NL. Colloid-in-liquid crystal gels formed via spinodal decomposition. Soft Matter. 10: 1602–1610. 2014. [PubMed: 24651134]
10. Kikuchi H, Yokota M, Hisakado Y, Yang H, Kajiyama T. Polymer-stabilized liquid crystal blue phases. Nature Mater. 1: 64–68. 2002. [PubMed: 12618852]
11. Xiang J, Lavrentovich OD. Blue-phase-polymer-templated nematic with sub-millisecond broad-temperature range electro-optic switching. Appl Phys Lett. 103: 051112. 2013;
12. Castles F, Morris SM, Hung JMC, Qasim MM, Wright AD, Nosheen S, Choi SS, Outram BI, Elston SJ, Burgess C, Hill L, Wilkinson TD, Coles HJ. Stretchable liquid-crystal blue phase gels. Nature Mater. 13: 817–821. 2014. [PubMed: 24880732]
13. Huck, WTS. Nanoscale assembly: chemical techniques. Springer; New York: 2005.
14. Zhao X, Pan F, Xu H, Yaseen M, Shan H, Hauser CAE, Zhang S, Lu JR. Molecular self-assembly and applications of designer peptide amphiphiles. Chem Soc Rev. 39: 3480–3498. 2010. [PubMed: 20498896]
15. Chakrabarty R, Mukherjee PS, Stang PJ. Supramolecular coordination: self-assembly of finite two- and three-dimensional ensembles. Chem Rev. 111: 6810–6918. 2011. [PubMed: 21863792]
16. de Gennes, PG, Prost, J. The physics of liquid crystals. Oxford science publications; Oxford: 1993.
17. Gu Y, Abbott NL. Observation of Saturn-ring defects around solid microspheres in nematic liquid crystals. Phys Rev Lett. 85: 4719–4722. 2000. [PubMed: 11082635]
18. Tkalec U, Ravnik M, Copar S, Zumer S, Musevic I. Reconfigurable knots and links in chiral nematic colloids. Science. 333: 62–65. 2011. [PubMed: 21719671]
19. Martinez A, Ravnik M, Lucero B, Visvanathan R, Zumer S, Smalyukh II. Mutually tangled colloidal knots and induced defect loops in nematic fields. Nature Mater. 13: 258–263. 2014. [PubMed: 24390381]
20. Mottram NJ, Sluckin TJ. Defect-induced melting in nematic liquid crystals. Liq Cryst. 27: 1301–1304. 2000.
21. Ravnik M, Zumer S. Landau-de Gennes modelling of nematic liquid crystal colloids. Liq Cryst. 36: 1201–1214. 2009.
22. Iliopoulos I, Wang TK, Audebert R. Viscometric evidence of interactions between hydrophobically modified poly(sodium acrylate) and sodium dodecyl-sulfate. Langmuir. 7: 617–619. 1991.

23. Hansson P, Lindman B. Surfactant-polymer interactions. Curr Opin Colloid Interface Sci. 1: 604–613. 1996.
24. Yekta A, Duhamel J, Brochard P, Adiwidjaja H, Winnik MA. A fluorescent-probe study of micelle-like cluster formation in aqueous-solutions of hydrophobically modified poly(ethylene oxide). Macromolecules. 26: 1829–1836. 1993.
25. Biggs S, Selb J, Candau F. Effect of surfactant on the solution properties of hydrophobically modified polyacrylamide. Langmuir. 8: 838–847. 1992.
26. Tanaka R, Meadows J, Williams PA, Phillips GO. Interaction of hydrophobically modified (hydroxyethyl) cellulose with various added surfactants. Macromolecules. 25: 1304–1310. 1992.
27. Guillemet F, Piculell L. Interactions in aqueous mixtures of hydrophobically-modified polyelectrolyte and oppositely charged surfactant- mixed micelle formation and associative phase separation. J Phys Chem. 99: 9201–9209. 1995.
28. Piculell L, Guillemet F, Thuresson K, Shubin V, Ericsson O. Binding of surfactants to hydrophobically modified polymers. Adv Colloid Interface Sci. 63: 1–21. 1996.
29. Mikhalyov I, Gretskaya N, Bergstrom F, Johansson LB. Electronic ground and excited state properties of dipyrromethene boron difluoride (BODIPY): dimers with application to biosciences. Phys Chem Chem Phys. 4: 5663–5670. 2002.
30. Yoon DK, Choi MC, Kim YH, Kim MW, Lavrentovich OD, Jung HT. Internal structure visualization and lithographic use of periodic toroidal holes in liquid crystals. Nature Mater. 6: 866–870. 2007. [PubMed: 17934466]
31. Pires D, Fleury J, Galerne Y. Colloid particles in the interaction field of a disclination line in a nematic phase. Phys Rev Lett. 98: 247801. 2007; [PubMed: 17677995]
32. Skarabot M, Ravnik M, Zumer S, Tkalec U, Poberaj I, Babic D, Musevic I. Hierarchical self-assembly of nematic colloidal superstructures. Phys Rev E. 77: 061706. 2008;
33. Fleury J, Pires D, Galerne Y. Self-connected 3D architecture of microwires. Phys Rev Lett. 103: 267801. 2009; [PubMed: 20366346]
34. Milette J, Relaix S, Lavigne C, Toader V, Cowling SJ, Saez IM, Lennox RB, Goodby JW, Reven L. Reversible long-range patterning of gold nanoparticles by smectic liquid crystals. Soft Matter. 8: 6593–6598. 2012.
35. Coursault D, Grand J, Zappone B, Ayeb H, Levi G, Felidj N, Lacaze E. Linear self-assembly of nanoparticles within liquid crystal defect arrays. Adv Mater. 24: 1461–1465. 2012. [PubMed: 22318807]
36. Voloschenko D, Pishnyak OP, Shiyanovskii SV, Lavrentovich OD. Effect of director distortions on morphologies of phase separation in liquid crystals. Phys Rev E. 65: 060701. 2002;
37. Higashiguchi K, Yasui K, Ozawa M, Odoi K, Kikuchi H. Spatial distribution control of polymer nanoparticles by liquid crystal disclinations. Polym J. 44: 632–638. 2012.
38. Karjiban RA, Shaari NS, Gunasakaran UV, Basri M. A coarse-grained molecular dynamics study of DLPC, DMPC, DPPC, and DSPC mixtures in aqueous solution. J Chem. 2013: 931051. 2013;
39. Hiemenz, PS, Rajagopalan, R. Principles of colloidal and surface chemistry. CRC; London: 1997.
40. Holmberg, K, Jonsson, B, Kronberg, B, Lindman, B. Surfactants and polymers in aqueous solution. Wiley; Chichester: 2003.
41. Abe A, Furuya H, Shimizu RN, Nam SY. Calculation of the conformation entropies of dimer liquid crystals and comparison with the observed transition entropies at constant volume. Macromolecules. 28: 96–103. 1995.
42. Israelachvili, JN. Intermolecular and surface forces. Elsevier; Oxford: 2011.
43. Nagarajan R, Ruckenstein E. Theory of surfactant self-assembly: a predictive molecular thermodynamic approach. Langmuir. 7: 2934–2969. 1991.
44. Ruckenstein E, Huber G, Hoffmann H. Surfactant aggregation in the presence of polymers. Langmuir. 3: 382–387. 1987.
45. Nagarajan R. Thermodynamics of nonionic polymer-micelle association. Colloids Surf. 13: 1–17. 1985.

46. Punnamaraju S, You H, Steckl AJ. Triggered release of molecules across droplet interface bilayer lipid membranes using photopolymerizable lipids. Langmuir. 28: 7657–7664. 2012. [PubMed: 22548362]

47. Iwata T, Suzuki K, Amaya N, Higuchi H, Masunaga H, Sasaki S, Kikuchi H. Control of cross-linking polymerization kinetics and polymer aggregated structure in polymer-stabilized liquid crystalline blue phases. Macromolecules. 42: 2002–2008. 2009.

48. Lin I, Miller DS, Bertics PJ, Murphy CJ, de Pablo JJ, Abbott NL. Endotoxin-induced structural transformations in liquid crystalline droplets. Science. 332: 1297–1300. 2011. [PubMed: 21596951]

49. Miller DS, Abbott NL. Influence of droplet size, pH and ionic strength on endotoxin-triggered ordering transitions in liquid crystalline droplets. Soft Matter. 9: 374–382. 2013. [PubMed: 23675387]

50. Dempsey GT, Vaughan JC, Chen KH, Bates M, Zhuang X. Evaluation of fluorophores for optical performance in localization-based super-resolution imaging. Nature Meth. 8: 1027–1040. 2011.

51. Gupta R, Muralidhara HS, Davis HT. Structure and phase behavior of phospholipid-based micelles in nonaqueous media. Langmuir. 17: 5176–5183. 2001.

52. Danino D, Gupta R, Satyavolu J, Talmon Y. Direct cryogenic-temperature transmission electron microscopy imaging of phospholipid aggregates in soybean oil. J Colloid Interface Sci. 249: 180–186. 2002. [PubMed: 16290584]

53. Salentinig S, Sagalowicz L, Leser ME, Tedeschi C, Glatter O. Transitions in the internal structure of lipid droplets during fat digestion. Soft Matter. 7: 650–661. 2011.

54. Kofiman N, Schnabel-Lubovsky M, Talmon Y. Nanostructure formation in the lecithin/isooctane/water system. J Phys Chem B. 117: 9558–9567. 2013. [PubMed: 23865978]

55. Lee HY, Hashizaki K, Diehn K, Raghavan SR. Reverse self-assembly of lipid onions induced by gadolinium and calcium ions. Soft Matter. 9: 200–207. 2013.

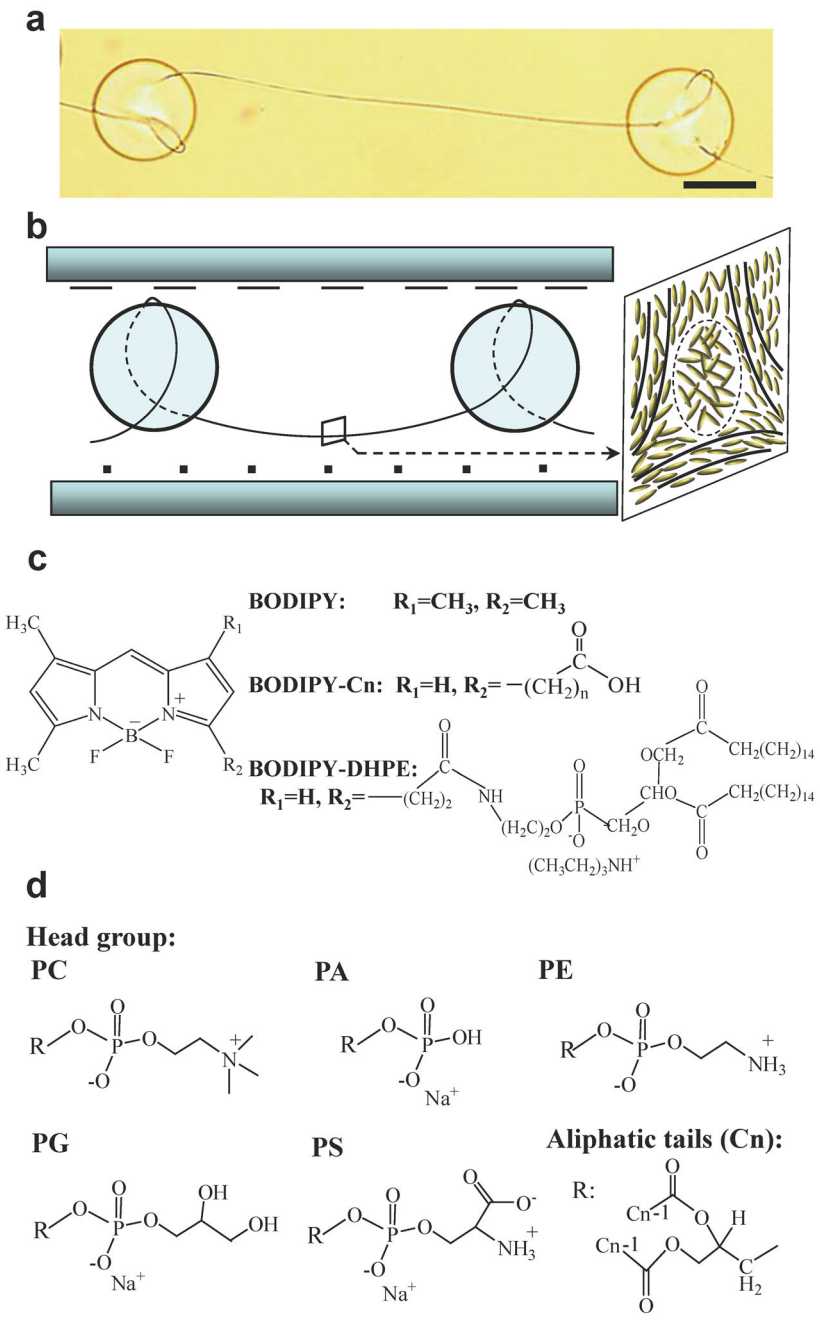

Figure 1. Disclination lines and amphiphiles

a,**b**, Bright field optical micrograph (**a**) and schematic illustration (**b**) of a singular line defect (disclination) of strength −1/2 formed around OTS-treated silica microparticles dispersed in a nematic LC with a 90° twist. Scale bar corresponds to 50 μm. Inset in (**b**) illustrates local ordering (solid line) of mesogens near the core of the −1/2 disclination (dashed circle). **c**,**d**, Molecular structures of BODIPY-amphiphiles (**c**) and phospholipids (PC-C*n*, in which *n* represents the number of methylene units in each aliphatic tail) (**d**) used in this study. PC: phosphatidylcholine; PA: phosphatidic acid; PE: phosphatidylethanolamine; PG: phosphatidylglycerol; PS: phosphatidylserine.

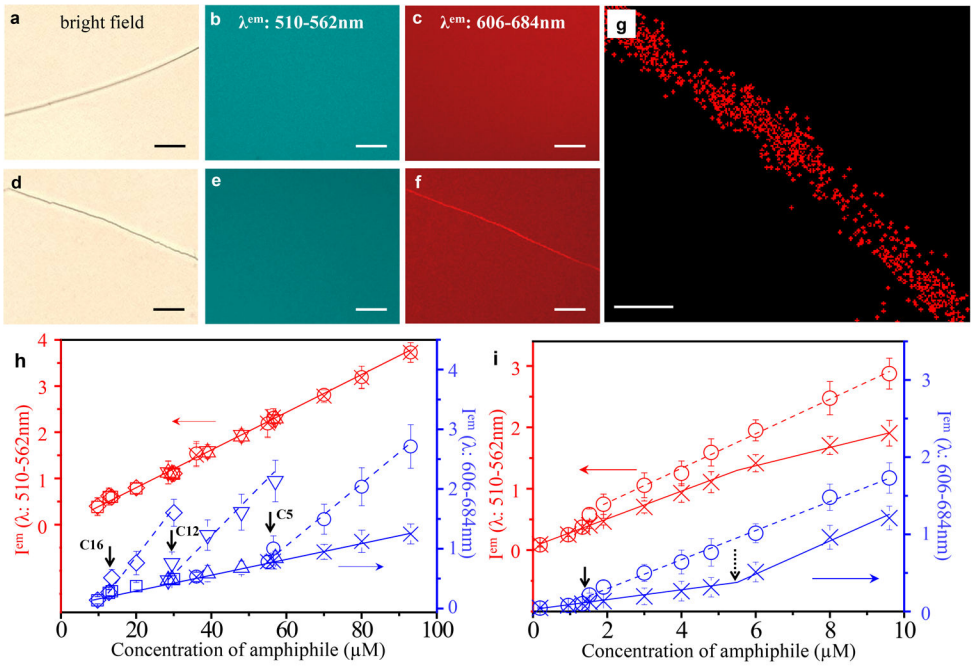

Figure 2. Self-assembly of amphiphiles in LC defects

a–**f**, Bright field micrograph of −1/2 disclination (**a**,**d**) and fluorescence micrographs (**b**,**e**: λ^{em} 510–562 nm; **c**,**f**: λ^{em} 606–684 nm) showing the distribution of BODIPY (**a**–**c**; 57 μM) or BODIPY-C5 (**d**–**f**; 59 μM) in and around the −1/2 disclination in nematic 5CB. Scale bars correspond to 20 μm. See Supplementary Information for exposure times. **g**, Super-resolution optical micrograph showing the distribution of PC-C12 (19 μM; doped with 10% mol/mol of ATTO 488-labeled PE-C14) within a disclination formed in nematic 5CB. Scale bar corresponds to 100 nm. **h**,**i**, Fluorescence intensity of BODIPY-amphiphiles (**h**; BODIPY-C5: ○ in defect, × in bulk; BODIPY-C12: ▽ in defect, △ in bulk; BODIPY-C16: ◇ in defect, □ in bulk) and BODIPY-DHPE (**i**; ○ in defect, × in bulk) in LC defects and the bulk nematic phase (λ^{em}: 510–562 nm (monomer): red; λ^{em}: 606–684 nm (dimer): blue). The solid and dashed lines are fits to the fluorescence intensity in the bulk phase and defect of the LC, respectively. The vertical solid arrows indicate the CAC of BODIPY-amphiphiles in defects. The vertical dashed arrow represents the CAC of BODIPY-DHPE in bulk LC. Error bars represent standard deviations and n=3 for each data point. One arbitrary unit represents 40,000 (left y-axis in (**h**)), 500 (right y-axis in (**h**)) or 400 (both y-axes in (**i**)) rescaled fluorescence intensity units (see Methods for details). The left y-axes were offset to avoid overlap of the monomeric and dimeric fluorescence signals.

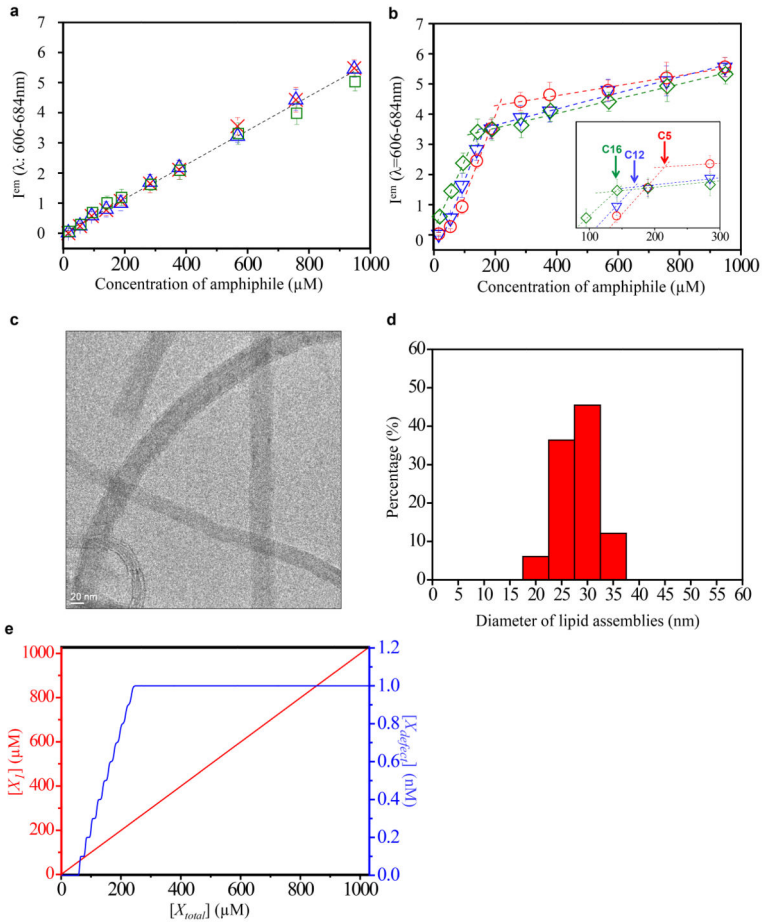

Figure 3. Controlled growth of assemblies in defects

a,**b**, Fluorescence intensity values for BODIPY-amphiphiles in bulk nematic phase (**a**) and LC defects (**b**). BODIPY-C5: ○ in defect, × in bulk; BODIPY-C12: ▽ in defect, △ in bulk; BODIPY-C16: ◇ in defect, □ in bulk. The dashed lines fit the fluorescence intensity in the LC bulk phase and defect region. Inset in (**b**) shows data in the concentration range of 80–300 μM. The vertical arrows in the inset indicate the concentration of BODIPY-amphiphiles (estimated from the intersection of best-fit lines above and below the threshold concentrations) at which there is a change in the mode of growth of the assemblies in the defects. Error bars represent standard deviations and n=6 for each data point. One arbitrary unit in (**a** and **b**) represents 1,000 rescaled fluorescence intensity units (see Methods for details). **c**, Cryo-TEM image of an amphiphilic assembly formed by PC-C12 in a blue phase LC. **d**, Histogram of diameters of lipid assemblies formed within LC defects. The histogram was assembled from 10 lipid assemblies in 3 independently prepared samples with 3 measurements of diameter recorded for each lipid assembly. **e**, Calculated dependence of the concentration of singly dispersed BODIPY-C5 ($[X_1]$) and self-assembled BODIPY-C5 ($[X_{defect}]$) on the total concentration of BODIPY-C5 ($[X_{total}]$), as predicted by equation (1).

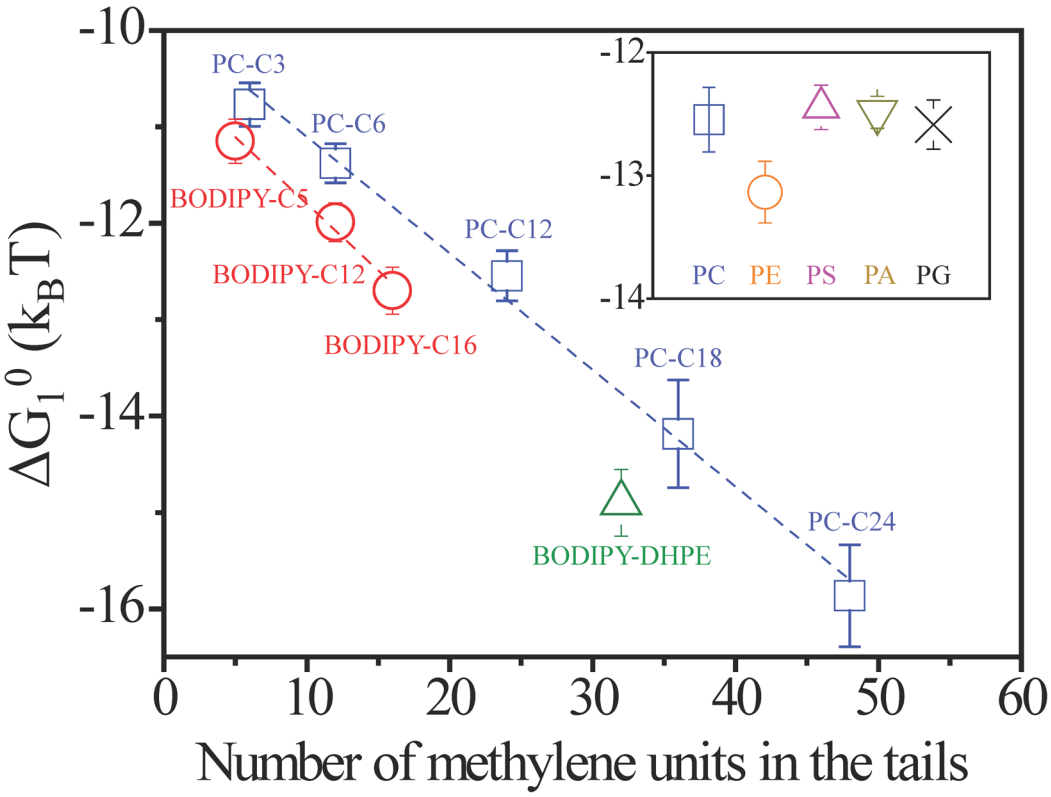

Figure 4. Dependence of standard free energy of self-assembly on amphiphile tail-length and head-group type

Standard free energy of transfer of a BODIPY-amphiphile or phospholipids (PC-C*n*, in which *n* represents the number of methylene units in each aliphatic tail) from a bulk LC phase into an assembly within a −1/2 line defect. The lines fit the data with a slope of −0.13 k_BT/methylene. Inset shows the standard free energy of transfer for C12 phospholipids with different head groups.

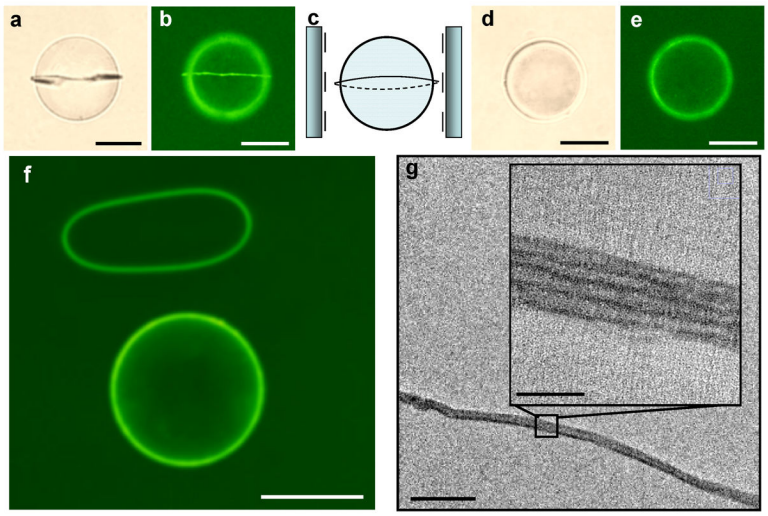

Figure 5. Reversible formation and in-situ cross-linking of molecular assemblies of amphiphiles templated by −1/2 “Saturn-ring” disclination line formed about microparticles

a–**e**, Bright field (**a** and **d**) and fluorescence micrographs (**b** and **e**) showing the distribution of photoreactive lipid diyne PC (20 μM; doped with 2 mol% of BODIPY-C5) in nematic 5CB (**a** and **b**) or isotropic 5CB (**d** and **e**). **c**, Schematic illustration of a −1/2 “Saturn-ring” defect around particles dispersed in nematic LC with 0° twist. **f**, Fluorescence microscope of a polymeric “o-ring” with a diameter of 20 nm that slipped from the equatorial plane of the microparticle. Scale bars correspond to 50 μm. **g**, TEM image of the polymeric structure obtained in **f**. Scale bar corresponds to 100 nm (inset: 20 nm).

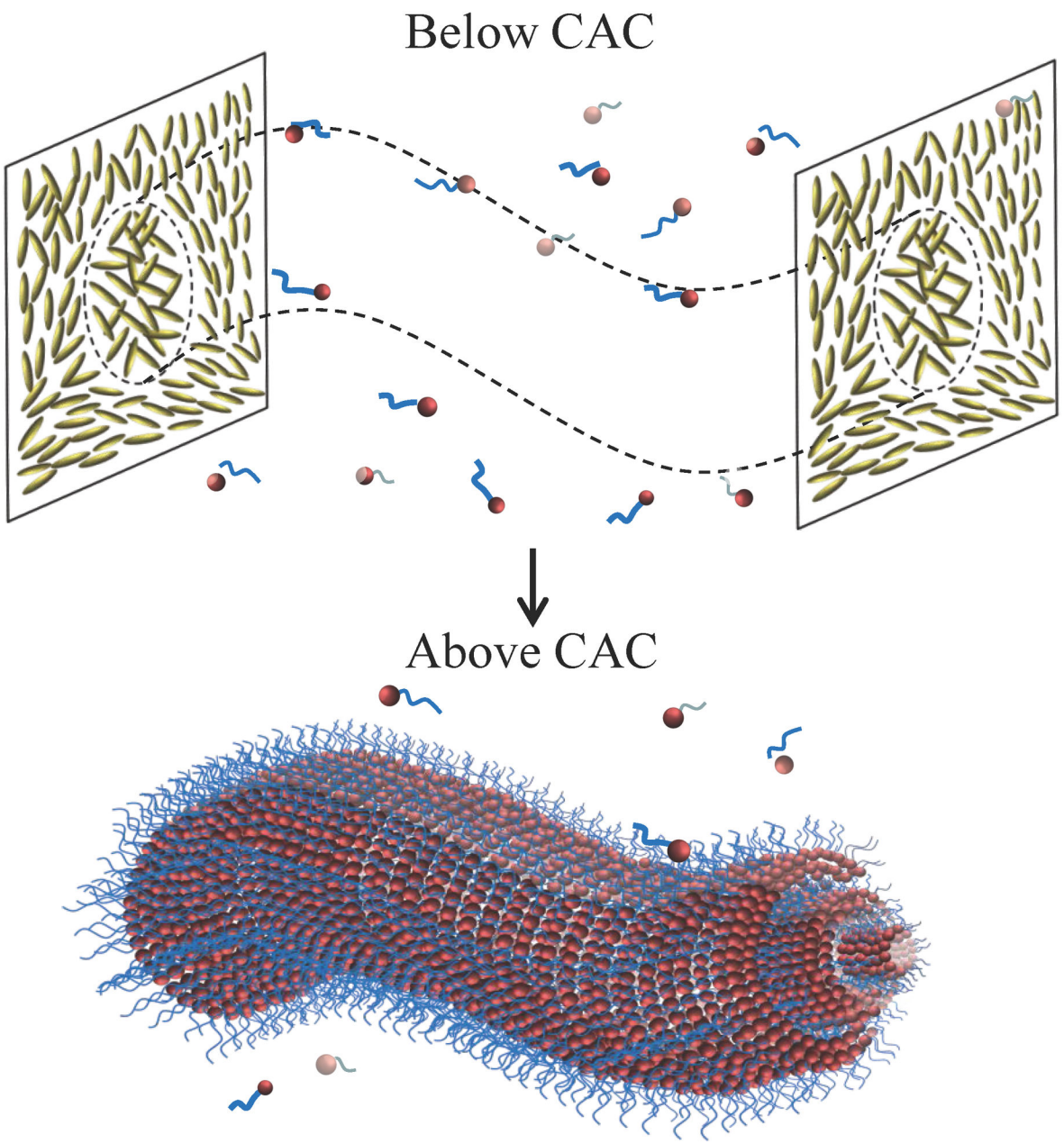

Figure 6.
Self-assembly of amphiphiles in LC defects.